Research Article | Vol. 13, No. 2 / 1 Feb 2022 / Biomedical Optics Express 875
Biomedical Optics EXPRESS

Impact of skin tone on photoacoustic oximetry and tools to minimize bias

YASH MANTRI[1] AND JESSE V. JOKERST[2,3,4,*]

[1]Department of Bioengineering, University of California San Diego, 9500 Gilman Drive, La Jolla, CA, 92093, USA
[2]Department of Nanoengineering, University of California San Diego, 9500 Gilman Drive, La Jolla, CA, 92093, USA
[3]Material Science Department, University of California San Diego, 9500 Gilman Drive, La Jolla, CA, 92093, USA
[4]Department of Radiology, University of California San Diego, 9500 Gilman Drive, La Jolla, CA, 92093, USA
[*]jjokerst@ucsd.edu

Abstract: The major optical absorbers in tissue are melanin and oxy/deoxy-hemoglobin, but the impact of skin tone and pigmentation on biomedical optics is still not completely understood or adequately addressed. Melanin largely governs skin tone with higher melanin concentration in subjects with darker skin tones. Recently, there has been extensive debate on the bias of pulse oximeters when used with darker subjects. Photoacoustic (PA) imaging can measure oxygen saturation similarly as pulse oximeters and could have value in studying this bias. More importantly, it can deconvolute the signal from the skin and underlying tissue. Here, we studied the impact of skin tone on PA signal generation, depth penetration, and oximetry. Our results show that subjects with darker skin tones exhibit significantly higher PA signal at the skin surface, reduced penetration depth, and lower oxygen saturation compared to subjects with lighter skin tones. We then suggest a simple way to compensate for these signal differences.

1. Introduction

Biomedical optics play an increasingly powerful role in human health, but the impact that skin tone and skin pigmentation have on optical imaging and diagnostics is not completely understood or adequately addressed. Melanin governs skin tone and is a strong light-absorbing pigment; thus, darker skin absorbs more photons leaving less light to probe the deeper tissues of interest. The primary challenge for optical medical devices is that variations in skin pigmentation can alter measurements between subjects in ways that the device was not designed to anticipate. Variable melanin content/skin tone has been reported to adversely affect the performance of a broad range of optical medical devices including pulse oximeters, [1] cerebral tissue oximeters, [2] hyperspectral reflectance imagers, [3] bilirubinometers, [4] wearable photoplethysmography, [5] other "wearables" in the consumer market (e.g., smart watches), [6,7] and photoacoustic (PA) imagers. [8] In one recent high-powered example, [1] 48,000 pulse oximetry readings in 8,675 white subjects and 1,326 black subjects were compared with arterial oxygen saturation measurements. The results, while controversial, [9] showed that Black subjects were 3.2-fold more likely to have undiagnosed hypoxemia, and potentially not get needed supplemental oxygen. This can lead to differences in health outcomes because Black people, Hispanics, and others often have darker skin tones. This disparity in health outcomes illustrates the importance of investigating the impact of skin pigmentation during, not after, medical device development.

Hypoxemia is an abnormal decrease in partial pressure of oxygen in the blood – a key parameter in clinical decision making in diseases including cancer, [10–12] COVID, [13,14] wound care, [15–17] chronic kidney disease, [18,19] aging, [20,21] *etc*. Measuring blood oxygen

#450224 https://doi.org/10.1364/BOE.450224
Journal © 2022 Received 1 Dec 2021; revised 13 Jan 2022; accepted 14 Jan 2022; published 20 Jan 2022

Biomedical Optics EXPRESS

saturation (sO_2) can be relatively straightforward due to the differences in absorption between oxy-and-deoxy-hemoglobin. But melanin is also a major optical absorber in tissue. Clinically, dermatologists use the Fitzpatrick scale to classify people with different skin tones. [22] The Fitzpatrick scale is a numerical classification system (1 (pale white) – 6 (black/very dark brown)) to estimate the response of different skin types to ultraviolet light (Fig. 1(A)). [23] Currently, few biomedical devices actively measure or compensate for changes in skin color between subjects.

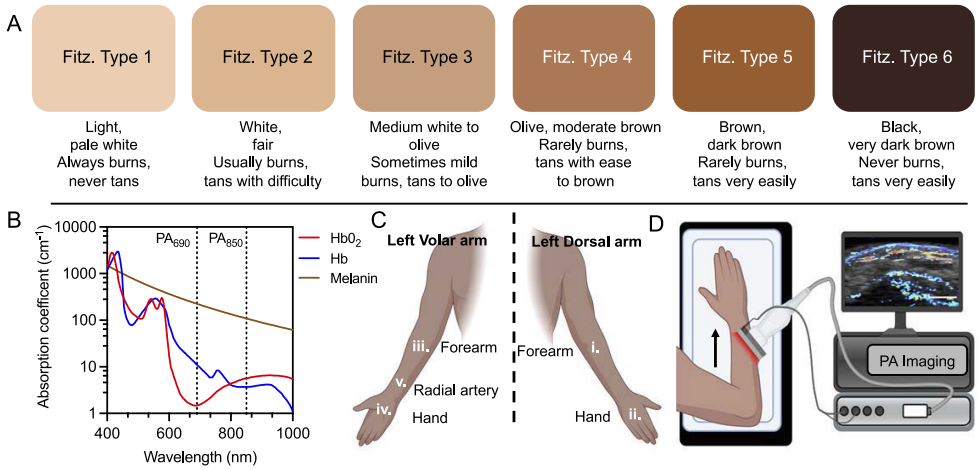

Fig. 1. Skin tone classification. A. Classification of skin tone based on the Fitzpatrick scale. [23] Fitzpatrick 1 is lightest and 6 is the darkest skin tone. **B.** Absorption coefficient (μa in cm^{-1}) of oxy-deoxyhemoglobin and melanin in the visible and near infrared region. Data from ref. [25] and [24]. PA imaging was done at 690 and 850 nm. **C.** Nine volunteers classified as Fitzpatrick 1, 4, and 6 were scanned at 5 locations on the left arm. **D.** Typical scan of the dorsal forearm using a handheld photoacoustic transducer. Arrow annotates the scan direction.

Tissue optical absorption is quantified by the local absorption coefficient ($\boldsymbol{\mu_a}$). A higher μ_a means that more photons are absorbed, which reduces the light penetrance into tissue. Tissue μ_a is a linear summation of the absorption of all chromophores present, weighed by chromophore concentration, Eq. (1). Here $\boldsymbol{\mu_a}$ denotes the absorption coefficient (cm^{-1}); $\boldsymbol{\lambda_i}$ is the imaging wavelength (nm); $\mathbf{HbO_2}$ and **Hb** denote oxy-and-deoxy-hemoglobin respectively. In tissue, $\boldsymbol{\mu_a}$ varies significantly with wavelength due to the inherent spectral absorption properties of constituent molecules like hemoglobin and melanin (Fig. 1(B)). [24,25] Other absorbing species in tissue include lipids, proteins, collagen, water *etc*. [26] But these have minimal absorption in the biological optical window (700–900 nm). [27,28] Many biomedical optics devices do not consider potential variation or uncertainty in $\mu_{a,skin}$ and thus unexpected differences in tissue light transport can compromise performance of optical technologies including pulse oximetry, fluorescence, PA, *etc*. [29]

$$\boldsymbol{\mu_{a,skin}}(\boldsymbol{\lambda_i}) = \mu_{a,HbO_2}(\lambda_i)[HbO_2] + \mu_{a,Hb}(\lambda_i)[Hb] + \mu_{a,melanin}(\lambda_i)[melanin] + \mu_{a,\,other\ absorbers}(\lambda_i)[other\ absorbers] \quad (1)$$

PA produces signal as a function of $\boldsymbol{\mu_a}$. [30] PA imaging delivers diffused light through tissue, where the photons are absorbed by dominant chromophores (hemoglobin and melanin) and converted to sound waves for acoustic imaging. [27,31] The intensity of PA signal is directly proportional to $\boldsymbol{\mu_a}$. [31] Vasculature and blood oxygen saturation (sO_2) can be mapped in 3D using multiple wavelengths. While many optical oximetry techniques offer an ensemble or point-based value of oxygenation, PA imaging offers a 3D map that can measure oxygenation

Biomedical Optics EXPRESS

through many centimeters of tissue. [32–35] Furthermore, PA can also deconvolute the skin layer from the tissue layer [36–38], and the first FDA-approved system was recently launched (Seno Medical). [39–41]

This work is an observational case series that aims to measure photoacoustic signal and oxygenation differences in healthy human subjects as a function of skin tone. We performed PA imaging and oximetry on nine healthy volunteers with a Fitzpatrick skin type of 1,4, and 6 (Fig. 1(C)-(D); n = 3 per skin type). [23] Our data shows significant changes in PA signal as a function of skin tone. Using the training data from the nine volunteers, we formulated a compensation equation that was tested on new Fitzpatrick type 3 and 5 subjects. Our case series shows that compensating for differences in skin tone is possible for photoacoustic oximetry.

2. Results

2.1. Effect of skin tone on surface photoacoustic signal

We imaged the dorsal and volar forearm and hand of nine subjects with Fitzpatrick skin type of 1, 4, and 6 (n = 3 each) (Table S1, Fig. 1(C)). The forearm and hand were selected because they have a relatively uniform distribution of melanin (Fig. S1), are relatively flat to facilitate scanning, and are relatively free of hair that can compromise imaging. Figure 2 shows the change in PA intensity as a function of Fitzpatrick skin type at 850 nm. PA intensity increases significantly ($p < 0.0001$, $R^2 = 0.81$) between Fitzpatrick scales 1–4 (104%) and 4–6 (47%). Subjects with darker skin tones showed considerably more streaking artifacts, noise, and clutter (Fig. 2(D-F and H)). [42] Within skin types, we observed significant changes ($p = 0.016$, Fitz. 4; $p = 0.008$, Fitz. 6) in PA intensity between the dorsal and volar hand of skin types 4 and 6 (at 850 nm) (Fig. S2). Dorsal areas were both darker and had higher signal. The dorsal and volar forearm within skin types 1, 4, and 6 showed no significant change ($p > 0.05$) in photoacoustic intensity, which is consistent with reports of similar melanin content in photo-protected skin. [43] The

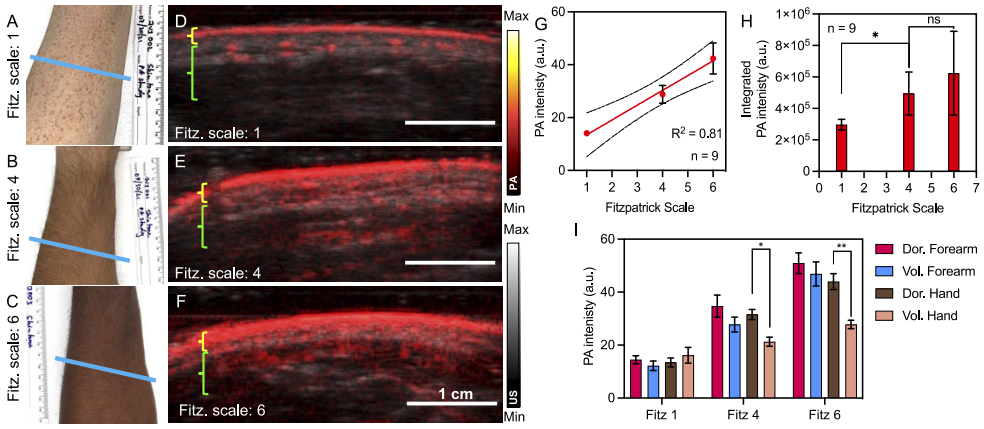

Fig. 2. Photoacoustic signal at 850 nm increases as a function of skin tone. A-C. Photographic images of the dorsal forearm of Fitzpatrick scale 1, 4, and 6 healthy volunteers. **D-F**. PA and US overlay from the blue imaging plane in A-C shows increase in PA signal and clutter from the skin surface. Yellow and green brackets mark skin and subdermal tissue respectively. **G.** PA intensity is linearly correlated with skin tone on the Fitzpatrick scale ($R^2 = 0.81$, n = 9). **H**. Integrated PA intensity of 1 cm subdermal tissue shows an increase in noise and clutter in subjects with darker skin tone. **I**. PA intensity is significantly different ($p < 0.05$) between dorsal and volar hand in the same group (Fitz 4, and 6 n = 3 each). Error bars represent standard deviation between the three subjects in each group, and scale bars in D-F denote 1 cm. These images were acquired on the LED-based PA system.

Biomedical Optics EXPRESS

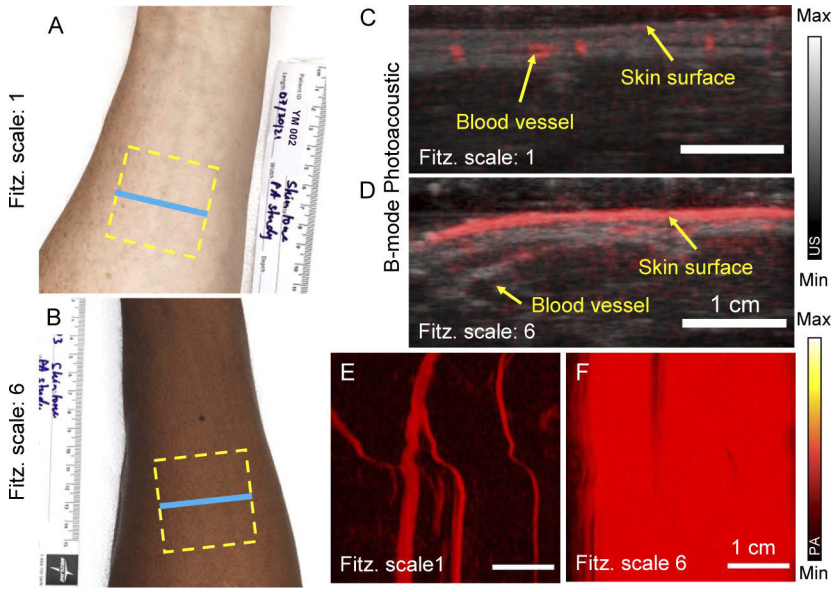

Fig. 3. High melanin in darker skin subjects obscures the underlying blood vessels in PA imaging (850 nm). A-B. Volar forearm of a Fitz. 1 and 6 subject respectively. Blue line are the planes imaged in panels **C/D. C.** Blood vessels are clearly visible in Fitz. 1 subject because light can penetrate through the skin. **D.** High melanin concentration in a Fitz. 6 subject reduces penetration depth and obscures underlying blood vessels which are visible on the US. **E-F.** Maximum intensity projection of all planes in the box shown as dashed square in **A/B** shows the map of blood vessels on a Fitz. 1 subject. The strong surface signal in the Fitz. 6 subject masks the vasculature underneath. These images were acquired on the LED-based PA system.

Table 1. Correction factors for PA oximetry for varying Fitzpatrick skin types.

Fitzpatrick Scale	Correction factor	Percent correction
1	0.99	–0.01%
2	1.029	2.9%
3	1.074	7.4%
4	1.118	11.8%
5	1.163	16.3%
6	1.207	20.7%

region-of-interest (ROI) outlines used for quantification can be found in the Supplement 1 (Fig. S3).

PA imaging at 690 nm also followed an increasing trend as a function of skin type ($p < 0.01$, $R^2 = 0.68$) (Fig. S3). Although the PA signal was consistently higher at 850 than 690 nm, this difference was not statistically significant ($p > 0.05$) (Fig. S3I). The slopes of PA intensity *vs.* Fitzpatrick scale at 850 and 690 nm have no significant difference ($p = 0.14$). Depth penetration into tissue was reduced at 690 nm as shorter wavelengths scatter more.

Biomedical Optics EXPRESS

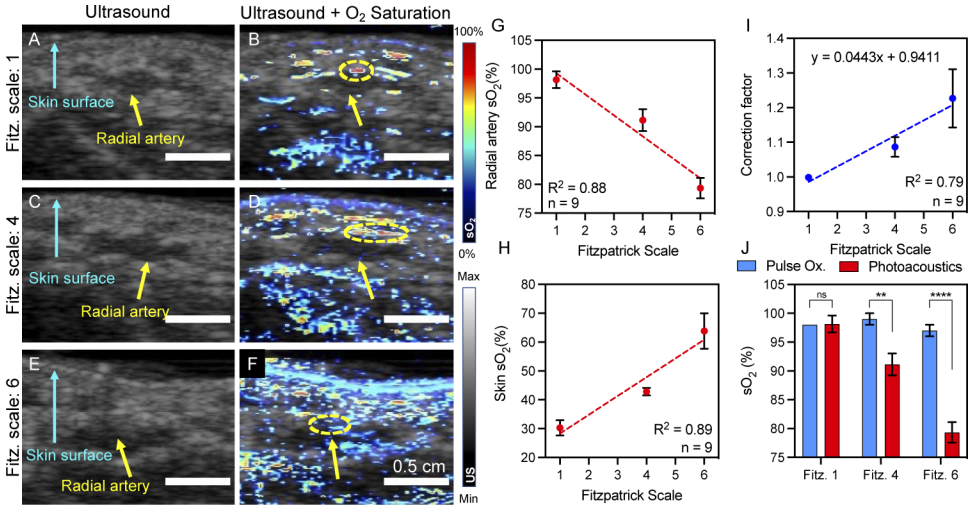

Fig. 4. Effect of skin tone on photoacoustic oximetry of the radial artery (690 and 850 nm). A-B. Low melanin concentration in Fitz. 1 subjects facilitates deeper and more accurate oxygen saturation measurements. **C-F.** An increase in melanin concentration in darker skin tones presents as high skin surface sO_2. The high skin signal reduces measurement accuracy in deeper blood vessels. Blue and yellow arrows point to the skin surface and radial artery respectively. Yellow dashed region in **B/D/F** represents the ROI used for s_aO_2 measurements. There is considerably more clutter and noise in darker skin toned subjects **D** and **F,** which obscures signal from the radial artery. **G.** PA measured oxygen saturation of the radial artery decreases linearly as a function of skin tone. **H.** The oxygen saturation on the skin surface increases linearly with increasing melanin concentration. **I.** The bias in the PA measurement can be compensated using a correction factor defined by the inset equation. **J.** The pulse oximeter shows no significant differences in sO_2 between different skin types contradicting the NEJM article. [1] But this study was done on a younger, healthier, and smaller cohort of patients. PA showed significant reduction in s_aO_2 for Fitz. 4 and 6 subjects due to increased melanin absorption at the skin surface. The pulse oximeter measures sO_2 peripherally where skin is thinnest compared to the radial artery where skin is considerably thicker. Scale bars measure 0.5 cm. error bars represent standard deviation between three subjects. These Images were acquired on the LED-based PA system.

2.2. *Effect of skin tone on photoacoustic depth penetration*

We also investigated the effect of skin tone on penetration depth to visualize deep blood vessels beneath the skin (Fig. 3). Blood vessels were easily mapped in the subject with Type 1 skin (Fig. 3(C) and (E)), but the high surface absorption in the Type 6 subject reduced light penetrance and thus contrast detectability of the underlying blood vessels (Fig. 3(D) and (F)). With the skin signal removed the signal-to-noise ratio for Fitz. 1 was 12.6 dB and Fitz. 6 was 3.2 dB (Fig. S4). Furthermore, a power analysis with 9 subjects and a null hypothesis that the true mean photoacoustic signal between each of the Fitzpatrick skin tone groups are equal shows 88% power in our study (alpha = 0.05, Fig. S5).

2.3. *Photoacoustic oximetry of the radial artery*

Clinically, the radial artery is a commonly used sampling site for blood gas measurements. [44] The radial artery should also include highly oxygenated blood in these healthy subjects (All subjects enrolled in this study had an sO_2 range between 96–100% measured via pulse oximetry (Table S1). Hence, we used PA imaging to non-invasively measure arterial sO_2 in

Biomedical Optics EXPRESS

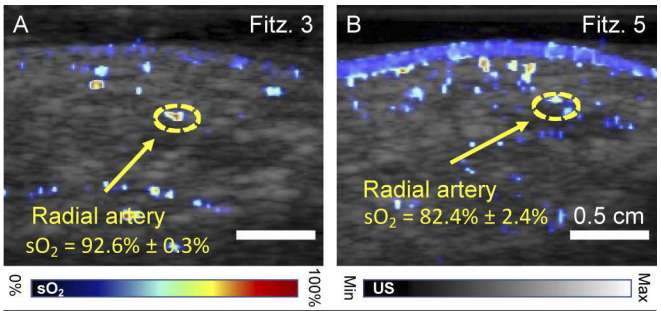

C

Skin type	Pulse Ox. sO_2	PA sO_2	Corrected sO_2	Percent Error
Fitz. 3	98 %	92.6 %	99.5 %	+ 1.53 %
Fitz. 5	98 %	82.4 %	95.8 %	- 2.24 %

Fig. 5. Compensating for differences in skin tone for photoacoustic oximetry. A-B. PA oximetry of the left radial artery in Fitz. 1 and 5 subjects respectively. The darker skin toned subject showed reduced sO_2 readings even though pulse oximetry measured 98% saturation in both cases. **C.** The previously defined correction factors were able to compensate for lack of signal in both subjects. Images were acquired at 690 and 850 nm. Standard deviation is measured over 30 frames. Yellow dotted circles outline the ROI for s_aO_2 quantification. Yellow arrow marks the radial artery. Scale bar measures 0.5 cm. These Images were acquired on the LED-based PA system.

the radial artery as a function of skin tone. The position of the radial artery was confirmed using doppler-ultrasound (Fig. S6), and arterial pulsation was visible on conventional grayscale ultrasound (US). We used a combination of 850 and 690 nm illumination on the LED-based PA system to measure oxygen saturation.

Subjects with darker skin tones showed significantly lower PA s_aO_2 (Fitz. 4: −7.98%; Fitz 6: 18.2%) compared to pulse oximetry ($p < 0.01$) (Fig. 4). The increase in melanin content in subjects with darker skin tones linearly increases the perceived sO_2 at the skin surface (Fig. 4(H)). The PA sO_2 measurements from the nine subjects were used as a training set to formulate a skin tone compensation equation (inset Fig. 4(I)). We assumed that the pulse oximeter readings were the ground truth and defined a correction factor to compensate for the deviated measurements using PA (Fig. 4(I)). The compensation factor was defined as a ratio between the pulse oximeter sO_2 (%)**:** PA measured s_aO_2 (%).

While a recent NEJM article showed a bias in pulse oximetry measurements, [1] in our case series, pulse oximeter measurements showed no significant differences between different Fitzpatrick skin types (Fig. 4(J)). This could be due to a small sample size and because we only measured young and healthy volunteers (mean age: 26.7 ± 3.7 years; BMI range: 19-24 kg/m^2). The PA sO_2 measurements were significantly lower compared to pulse oximetry for darker skin types ($p < 0.01$) (4 and 6, Fig. 4(J))

2.4. Compensating for differences in skin tone for photoacoustic oximetry

The equation in Fig. 4(I) defined the correction factor for all Fitzpatrick skin types listed in Table 1. We tested these values in 2 new subjects with a Fitzpatrick rating of 3 and 5 (Fig. 5).

Biomedical Optics EXPRESS

The darker Fitzpatrick type 5 subject showed a significantly lower s_aO_2 reading compared to the lighter Fitzpatrick type 3 subject ($p < 0.001$). Using the correction factors defined in Table 1, we were able to compensate for skin absorption and amend measurements to within ±2.24% error compared to the pulse oximeter (Fig. 5(C)). The corrected sO_2 is a product of the PA s_aO_2 and the correction factor for the Fitzpatrick skin type.

2.5. Difference in LED or Laser-based photoacoustics

Finally, we studied the effect of the illumination source (LED *vs.* laser) on photoacoustic evaluation of different skin tones. The LED source operates at a 100-200-fold lower energy compared to the laser. [45] The laser-based PA of the skin surface showed a positive correlation ($R^2 = 0.70$, $p < 0.001$) similar to the LED-based PA. There was a 12.5% and 71.1% increase in PA signal between Fitzpatrick type 1–4 and 4–6 subjects respectively (Fig. S7).

PA oximetry using the laser-based system was done at 850 and 750 nm. The sO_2 measurements are independent of the imaging wavelengths. Like the LED system, the laser-based system also showed a decrease in radial artery oxygenation for darker subjects (Fig. S8). The absorption by melanin in the Fitzpatrick type 6 subject was so high that the PA s_aO_2 dropped to 1.3%. The Fitzpatrick 1 subject also showed a lower s_aO_2 (59.2%) in comparison to the LED-system (97.8%). This could be because of the reconstruction algorithms used to reduce noise and calculate sO_2. [46]

3. Discussion

The young and healthy subjects recruited in this study had no previous history of cardiovascular disorders and were not on any medications that altered their oxygenation and perfusion status. Hence, the main significant difference between subjects with varying Fitzpatrick skin types was the concentration of melanin in their skin. Melanosomes are subcellular organelles that synthesize and store melanin. Studies have shown that subjects with darker skin tones have significantly more isolated, larger, and higher concentrations of melanosomes than subjects with lighter skin tones. [47,48] The larger and more concentrated melanosomes increase the absorption cross section of melanin resulting in enhanced light absorption (higher $\boldsymbol{\mu_a}$ of melanin in Eq. (1). The increase in melanin μ_a leads to higher PA signal at the skin surface and reduced depth penetration. Furthermore, larger melanosomes in darker subjects (1.44 ± 0.67 μm^2, from Thong *et al.* [48]) tend to scatter more near infrared light (NIR) than smaller melanosomes (0.94 ± 0.48 μm^2, from Thong *et al.* [48]) found in lighter skin toned patients.

PA imaging relies heavily on NIR illumination, [49] and thus increased scattering in this region further impedes light penetration through tissue. [50] With fewer photons making it through the skin in darker subjects, PA depth penetration is also reduced. The strong skin absorption and PA in Fitzpatrick type 6 subjects makes it difficult to visualize underlying vasculature (Fig. 3(D)/F). Even in Fitzpatrick 1 subjects, PA imaging with 690 nm did not penetrate deeper than the skin surface (Fig. S3D) as melanin has a higher $\boldsymbol{\mu_a}$ at 690 nm (Fig. 1(B)). [24] Time gain compensation to boost deeper signals coupled with noise reduction algorithms could help perform deeper PA imaging. [51] The smaller melanosomes in darker subjects could also enhance PA by increasing the surface area to volume ratio of the melanosomes. (Increasing surface-area-to-volume ratios is known to result in PA enhancement. [31,52])

The increase in PA at the skin surface in darker subjects results in streaking and clutter artifacts (Fig. 2(D)-(F)). Although there is reduced light penetrance through the skin, subdermal (1 cm under skin surface) PA signal is significantly higher in Fitzpatrick type 6 than type 1 subjects ($p < 0.01$). The increased subdermal PA signal is attributed to streaking and clutter artifacts. The use of a single linear array of transducers and the presence of strong absorbers like melanin in darker subjects results in streaking artifacts. [42] Streaking artifacts can be reduced using filtered back projection or PA computed tomography. [53] Clutter is a phenomenon caused by

Biomedical Optics EXPRESS

multipath reverberations or off-axis scatterers. It leads to a static cloud of echo signals occluding the tissue regions of interest. [42,54,55] Higher PA signal in darker subjects leads to stronger reverberations and increased clutter in subdermal tissue. Furthermore, streaking and clutter cloak physiological PA signals from blood vessels making it difficult to differentiate between signal and noise (Fig. 2(E)-(F)). This cloaking is only exacerbated during PA oximetry that combines data from two wavelengths (Fig. 4(B/D/F)). Fluence correction, [56] plane wave ultrasound from different angles, [57] focused ultrasound, [58] spatial weighting, [59] and deep learning [45] have shown promise in reducing noise and clutter in PA images.

The sO_2 measurements are dependent on PA signal at both 850 and 690 nm, the lack of PA depth penetration at 690 nm results in erroneous sO_2 readings. Furthermore, the increase in clutter and noise in darker skin toned subjects also interferes with their s_aO_2 evaluation (Fig. 4(B, D, and F)). The clutter in Fitzpatrick type 4 and 6 subjects makes ROI analysis difficult. Due to these perturbations, darker skin toned subjects show false signs of hypoxemia.

Pulse oximetry is a cheap, quick, and non-invasive oxygenation measurement technique but is limited to only peripheral sO_2 measurements where skin is relatively thin. [60] The arterial blood gas test is the most accurate way of determining the partial pressure of oxygen in blood, but is an invasive technique often resulting in various complications ranging from spasms, occlusions, infections *etc*. [61] PA imaging is advantageous because it is provides non-invasive local oxygen saturation and tissue perfusion map in real time. It is important to assess oxygen saturation locally to better understand the diseased state and to take more informed clinical decisions.

Other optical oximetry techniques such as pulse oximeters are often calibrated with a wide range of skin types, but the measurement inherently discards the concentration and $\boldsymbol{\mu_a}$ of melanin and other absorbers in Eq. (1), resulting in erroneous readings. [62,63] Although a short case series, this study shows that skin tone has a significant impact on the interaction of light with tissue, and that it must be studied in more detail.

Compensating for the under reporting of s_aO_2 in higher Fitzpatrick skin type subjects is a critical finding. The equation and correction factors in Fig. 4 and Table 1 represent a small cohort of subjects. Nevertheless, this proof-of-concept study shows that compensating for different skin tones could be as simple as a software update for these imaging systems. Future work will evaluate these conclusions in larger cohorts including subjects with arterial blood gas measurements. Ideally, we would objectively measure skin color using a colorimeter or reflectance spectroscopy before any clinical measurements. [64] This color measurement would further inform the image processing tool to compensate for changes in signal due to skin color by changing the weights for PA signal at each imaging wavelength.

Finally, the difference in oximetry results using the LED-based and laser-based systems could be explained by the different absorption spectra of oxy-deoxy-hemoglobin used by these commercial systems. [46] The laser-based system consistently under reports oxygenation values, but follows the same trends of decreasing s_aO_2 as a function of Fitzpatrick skin type.

4. Methods

4.1. Subjects

This work was performed in compliance with the ethical rules for human experimentation stated in the 1975 Declaration of Helsinki and approved by the University of California San Diego's Human Research Protections program. Eleven volunteers were recruited for this study. Subjects signed an informed written consent prior to participation. Inclusion criteria were (i) subjects >18 years old and able to provide informed written consent, (ii) pulse oximetry reading >96% on the left index finger at rest, [65] and (iii) a body mass index ranging from 18.5–25 kg/m^2. [66] Exclusion criteria were (i) subjects with known cardiovascular disease history, (ii) on medications that alter hemodynamic status such as blood pressure, oxygenation *etc*. (iii) presence of wounds in the imaging area, and (iv) previous history of skin disorders.

Biomedical Optics EXPRESS

All subjects were scanned over five locations on the left arm: (i) dorsal forearm, (ii) dorsal hand, (iii) volar forearm, (iv) volar hand, and (v) radial artery. An area measuring approximately 4 cm x 3 cm was scanned at imaging spots i – iv. The radial artery oxygenation was scanned in a single imaging plane. Before scanning, the imaging area was cleaned using alcohol. Pulse oximetry was done using a finger pulse oximeter from ZAcurate, Texas, USA. Subjects were classified into different Fitzpatrick skin types subjectively by Y.M. and objectively using the ITA scale. The calculations for determining ITA score can be found elsewhere. [67] The skin color quantification was done using a commercially available WR10QC portable colorimeter from Fru, China. The colorimeter used a D65 light source, CIE 10° observer, and measured CIEL*a*b color space.

4.2. Photoacoustic–ultrasound imaging

We used two commercially available PA imaging systems: one LED-based and one laser-based. The LED-based system was the AcousticX from Cyberdyne Inc., Tsukuba, Japan. The AcousticX system uses two LED-arrays operating with a pulse width of 70 ns and 4 KHz repetition rate. The illumination wavelengths used for imaging points i – iv were 850 and 690 nm separately. The radial artery was imaged using a combination of 850 and 690 nm illumination to measure oxygen saturation. The AcousticX employs a 128-element ultrasound transducer operating at a central frequency of 9 MHz, bandwidth of 80.9%, and with a 4-cm field-of-view. We used the proprietary AcousticX software for image acquisition and visualization.

The laser-based system was the VisualSonics Vevo 2100 LAZR from FUJIFILM VisualSonics Inc., Toronto, Canada. We scanned with a LZ250 transducer with a central frequency of 21 MHz. Images were acquired at 850 and 690 nm. PA spectra was acquired between 680–970 nm with a step size of 2 nm. PA oximetry was carried out using the in-built OxyHemo function using 750 and 850 nm illumination. Doppler imaging on this system was used to confirm the position of the radial artery.

We used sterile ultrasound coupling gel (Aquasonic 100, Parker Laboratories Inc. Fairfield NJ, USA) for coupling with the skin surface. All images were acquired at 30 frames/s. Image acquisition settings such as gain, dynamic range, and averaging were kept consistent for each machine between all Fitzpatrick skin types. A minimum of 80 frames were acquired for each scan. All scans were done using a hand-held transducer in a proximal-distal direction.

4.3. Image processing

All the image processing was done using Fiji, an ImageJ extension, version 2.1.0/1.53c. Data was plotted using Prism version 9.0.0. A minimum of 80 frames were processed for each scan. For the two wavelengths (690 and 850 nm), we processed a minimum of 640 frames for regions i-iv. For the radial artery, a minimum of 30 frames were acquired. Both the LED and laser-based systems acquire oximetry images in a step-by-step function of PA at wavelength 1–2 followed by B-mode US. Internally, the processing is done using a pixel-by-pixel analysis using the manufacturer's software and algorithms. The LED-based system does offer more control over weighing signal from each wavelength and the extinction coefficients of oxy-deoxy-hemoglobin that can help to correct for differences in skin absorption.

Data was quantified using custom ROI analysis for each 80-frame scan. We drew ROIs for skin signal generation as shown in Fig. S3. The ROI outline followed the contour of the skin, and we quantified the mean PA intensity within the ROI. We were careful to include only the skin surface using the B-mode US. The ROI was dynamically changed for every frame of the scan. To quantify subdermal PA signal, we drew a standard ROI measuring 1 cm deep and 4 cm wide. This ROI was held constant throughout the 80 frames while ensuring exclusion of the skin surface. We quantified the integrated PA intensity, i.e., the sum of all pixel intensities within the

Biomedical Optics EXPRESS

ROI. The integrated intensity was chosen to quantify net noise and clutter, and reduce the effect of dark pixels on the PA.

To measure oxygen saturation, we drew custom ROIs on the oximetry images taken under default settings from both scanners. We averaged the s_aO_2 across 30 frames. PA at the superior edge of the vessel was representative of the arterial sO_2 (Fig. 4).

The compensation equation was formed by plotting the compensation factor *vs.* the Fitzpatrick scale. The compensation factor was defined as the ratio between pulse oximetry sO_2 and PA s_aO_2. We calculated a unique compensation factor for each subject. The compensation factor for each skin type was an average of three subjects. The correction factors for all the Fitzpatrick types were calculated by solving the compensation equation. The correction factors were then tested on two new subjects (Fitzpatrick types 3 and 5).

4.4. Statistics

The error bars in all plots represents standard deviation. Standard deviation in grouped analysis of $n = 9$ for Fitzpatrick types 1, 4, and 6 (3 each) was propagated from each patient where we quantified a minimum of 80-frames each. A simple linear regression was fit to the data measuring changes in PA signal and s_aO_2 as a function of Fitzpatrick skin type. All significance testing was done using a 2-tailed, unpaired student's t-test; p-value < 0.05 was considered significant.

5. Conclusion

The effect of skin tone on PA imaging was explored in this study. Our findings show that subjects with darker skin tones show increased absorption of light at the skin surface. This increase in surface absorption leads to reduced penetration depth and obscures underlying blood vessels. PA imaging is an ideal tool to study the transportation of light through tissue, because it can deconvolute signal from the skin surface. PA oximetry of the radial artery showed that under the same imaging conditions, subjects with darker skin tones exhibit lower arterial oxygen saturation. This technical bias was attributed to the increase in melanin concentration in darker subjects. The bias against darker skin toned subjects could be easily corrected by formulating an equation describing the change in oxygen saturation as a function of Fitzpatrick skin type. This correcting equation was able to compensate for the reduced PA signal in two test subjects with <2% error compared to pulse oximeter readings. Finally, the use of two independent PA systems confirmed our trends and showed that the laser-based system had an even more profound impact on PA oximetry compared to the LED-based system.

Funding. University of California, San Diego (Galvanizing Engineering in Medicine program); National Institutes of Health (S10 OD021821); National Institute on Aging (R21 AG065776).

Acknowledgements. Figure 1(C-D) and Fig. S1A were made using BioRender.com. We thank all the study participants for their time and patience.

Disclosures. There are no conflicts to declare.

Data Availability. Data underlying the results presented in this paper are not publicly available at this time but may be obtained from the authors upon reasonable request.

Supplemental document. See Supplement 1 for supporting content.

References

1. M. W. Sjoding, R. P. Dickson, T. J. Iwashyna, S. E. Gay, and T. S. Valley, "Racial bias in pulse oximetry measurement," N. Engl. J. Med. **383**(25), 2477–2478 (2020).
2. P. E. Bickler, J. R. Feiner, and M. D. Rollins, "Factors affecting the performance of 5 cerebral oximeters during hypoxia in healthy volunteers," Anesth. Analg. **117**(4), 813–823 (2013).
3. M. J. Mendenhall, A. S. Nunez, and R. K. Martin, "Human skin detection in the visible and near infrared," Appl. Opt. **54**(35), 10559–10570 (2015).
4. P. Szabo, M. Wolf, H. U. Bucher, J. C. Fauchere, D. Haensse, and R. Arlettaz, "Detection of hyperbilirubinaemia in jaundiced full-term neonates by eye or by bilirubinometer?" Eur. J. Pediatr. **163**(12), 722–727 (2004).

Biomedical Optics EXPRESS

5. A. Shcherbina, C. M. Mattsson, D. Waggott, H. Salisbury, J. W. Christle, T. Hastie, M. T. Wheeler, and E. A. Ashley, "Accuracy in wrist-worn, sensor-based measurements of heart rate and energy expenditure in a diverse cohort," J. Pers. Med. **7**(2), 3 (2017).
6. P. J. Colvonen, P. N. DeYoung, N.-O. A. Bosompra, and R. L. Owens, "Limiting racial disparities and bias for wearable devices in health science research" (Oxford University US, 2020).
7. P. J. Colvonen, "Response To: Investigating sources of inaccuracy in wearable optical heart rate sensors," NPJ Digit. Med. **4**(1), 38 (2021).
8. X. Li, U. S. Dinish, J. Aguirre, R. Bi, K. Dev, A. B. E. Attia, S. Nitkunanantharajah, Q. H. Lim, M. Schwarz, Y. W. Yew, S. T. G. Thng, V. Ntziachristos, and M. Olivo, "Optoacoustic mesoscopy analysis and quantitative estimation of specific imaging metrics in Fitzpatrick skin phototypes II to V," J. Biophotonics **12**(9), e201800442 (2019).
9. J. Kiani, "Pulse oximeters are not racist," Neonatology Today **16**, 143–144 (2021).
10. M. C. Brahimi-Horn, J. Chiche, and J. Pouysségur, "Hypoxia and cancer," J. Mol. Med. **85**(12), 1301–1307 (2007).
11. V. Bhandari, C. Hoey, L. Y. Liu, E. Lalonde, J. Ray, J. Livingstone, R. Lesurf, Y.-J. Shiah, T. Vujcic, and X. Huang, "Molecular landmarks of tumor hypoxia across cancer types," Nat. Genet. **51**(2), 308–318 (2019).
12. K. Graham and E. Unger, "Overcoming tumor hypoxia as a barrier to radiotherapy, chemotherapy and immunotherapy in cancer treatment," Int. J. Nanomed. **13**, 6049–6058 (2018).
13. K. B. Kashani, "Hypoxia in COVID-19: sign of severity or cause for poor outcomes," in *Mayo Clinic Proceedings* (Elsevier, 2020), 1094–1096.
14. N. Shenoy, R. Luchtel, and P. Gulani, "Considerations for target oxygen saturation in COVID-19 patients: are we under-shooting?" BMC Med. **18**(1), 260 (2020).
15. M. A. Howard, R. Asmis, K. K. Evans, and T. A. Mustoe, "Oxygen and wound care: a review of current therapeutic modalities and future direction," Wound Repair Regen. **21**(4), 503–511 (2013).
16. W. X. Hong, M. S. Hu, M. Esquivel, G. Y. Liang, R. C. Rennert, A. McArdle, K. J. Paik, D. Duscher, G. C. Gurtner, and H. P. Lorenz, "The role of hypoxia-inducible factor in wound healing," Adv. Wound Care **3**(5), 390–399 (2014).
17. L. MacCarthy-Morrogh and P. Martin, "The hallmarks of cancer are also the hallmarks of wound healing," Sci. Signaling **13**(648), 1 (2020).
18. Q. Fu, S. P. Colgan, and C. S. Shelley, "Hypoxia: the force that drives chronic kidney disease," Clin. Med. Res. **14**(1), 15–39 (2016).
19. F. Locatelli, S. Fishbane, G. A. Block, and I. C. Macdougall, "Targeting hypoxia-inducible factors for the treatment of anemia in chronic kidney disease patients," Am. J. Nephrol. **45**(3), 187–199 (2017).
20. E.-J. Yeo, "Hypoxia and aging," Exp. Mol. Med. **51**(6), 1–15 (2019).
21. J. Burtscher, R. T. Mallet, M. Burtscher, and G. P. Millet, "Hypoxia and brain aging: neurodegeneration or neuroprotection?" Ageing Res. Rev. **68**, 101343 (2021).
22. S. Sachdeva, "Fitzpatrick skin typing: Applications in dermatology," Indian J. Dermatol. Venereol. Leprol. **75**(1), 93 (2009).
23. J. D'Orazio, S. Jarrett, A. Amaro-Ortiz, and T. Scott, "UV radiation and the skin," Int. J. Mol. Sci. **14**(6), 12222–12248 (2013).
24. S. L. Jacques, "Melanosome absorption coefficient," Oregon Medical Laser Center, 7 (1998).
25. S. Prahl, "Optical absorption of hemoglobin," http://omlcogi.edu/spectra/hemoglobin (1999).
26. M. Omar, J. Aguirre, and V. Ntziachristos, "Optoacoustic mesoscopy for biomedicine," Nat. Biomed. Eng. **3**(5), 354–370 (2019).
27. M. Xu and L. V. Wang, "Photoacoustic imaging in biomedicine," Rev. Sci. Instrum. **77**(4), 041101 (2006).
28. L. V. Wang and H.-i. Wu, *Biomedical Optics: Principles and Imaging* (John Wiley & Sons, 2012).
29. E. Vienneau, T. Vu, and J. Yao, "Photoacoustic imaging of skin," *Imaging Technologies and Transdermal Delivery in Skin Disorders* (Wiley, 2019), pp. 411–442.
30. S. Manohar and D. Razansky, "Photoacoustics: a historical review," Adv. Opt. Photonics **8**(4), 586–617 (2016).
31. Y. Mantri and J. V. Jokerst, "Engineering plasmonic nanoparticles for enhanced photoacoustic imaging," ACS Nano **14**(8), 9408–9422 (2020).
32. E. Zhang, J. Laufer, R. Pedley, and P. Beard, "In vivo high-resolution 3D photoacoustic imaging of superficial vascular anatomy," Phys. Med. Biol. **54**(4), 1035–1046 (2009).
33. Y. Mantri, J. Tsujimoto, B. Donovan, C. C. Fernandes, P. S. Garimella, W. F. Penny, C. A. Anderson, and J. V. Jokerst, "Photoacoustic monitoring of angiogenesis predicts response to therapy in healing wounds," medRxiv, 2021.2010.2013.21264867 (2021).
34. A. Hariri, J. Wang, Y. Kim, A. Jhunjhunwala, D. L. Chao, and J. V. Jokerst, "In vivo photoacoustic imaging of chorioretinal oxygen gradients," J. Biomed. Opt. **23**(03), 1 (2018).
35. B. Hindelang, J. Aguirre, A. Berezhnoi, H. He, K. Eyerich, V. Ntziachristos, T. Biedermann, and U. Darsow, "Optoacoustic mesoscopy shows potential to increase accuracy of allergy patch testing," Contact Dermatitis **83**(3), 206–214 (2020).
36. C. Moore and J. V. Jokerst, "Strategies for image-guided therapy, surgery, and drug delivery using photoacoustic imaging," Theranostics **9**(6), 1550–1571 (2019).
37. A. Hariri, F. Chen, C. Moore, and J. V. Jokerst, "Noninvasive staging of pressure ulcers using photoacoustic imaging," Wound Rep. Reg. **27**(5), 488–496 (2019).

Biomedical Optics EXPRESS

38. S. Agrawal, M. Kuniyil Ajith Singh, K. Johnstonbaugh, D. C. Han, C. R. Pameijer, and S.-R. Kothapalli, "Photoacoustic imaging of human vasculature using LED versus laser illumination: A comparison study on tissue phantoms and in vivo humans," Sensors **21**(2), 424 (2021).
39. B. E. Dogan, G. L. Menezes, R. S. Butler, E. I. Neuschler, R. Aitchison, P. T. Lavin, F. L. Tucker, S. R. Grobmyer, P. M. Otto, and A. T. Stavros, "Optoacoustic imaging and gray-scale US features of breast cancers: correlation with molecular subtypes," Radiology **292**(3), 564–572 (2019).
40. E. I. Neuschler, R. Butler, C. A. Young, L. D. Barke, M. L. Bertrand, M. Böhm-Vélez, S. Destounis, P. Donlan, S. R. Grobmyer, and J. Katzen, "A pivotal study of optoacoustic imaging to diagnose benign and malignant breast masses: a new evaluation tool for radiologists," Radiology **287**(2), 398–412 (2018).
41. G. L. Menezes, R. M. Pijnappel, C. Meeuwis, R. Bisschops, J. Veltman, P. T. Lavin, M. J. Van De Vijver, and R. M. Mann, "Downgrading of breast masses suspicious for cancer by using optoacoustic breast imaging," Radiology **288**(2), 355–365 (2018).
42. W. C. Vogt, C. Jia, K. A. Wear, B. S. Garra, and T. J. Pfefer, "Phantom-based image quality test methods for photoacoustic imaging systems," J. Biomed. Opt. **22**(9), 1–14 (2017).
43. S. Alaluf, D. Atkins, K. Barrett, M. Blount, N. Carter, and A. Heath, "Ethnic variation in melanin content and composition in photoexposed and photoprotected human skin," Pigm. Cell Res. **15**(2), 112–118 (2002).
44. S. P. Dev, M. D. Hillmer, and M. Ferri, "Arterial puncture for blood gas analysis," N. Engl. J. Med. **364**(5), e7 (2011).
45. A. Hariri, K. Alipour, Y. Mantri, J. P. Schulze, and J. V. Jokerst, "Deep learning improves contrast in low-fluence photoacoustic imaging," Biomed. Opt. Express **11**(6), 3360–3373 (2020).
46. M. Gehrung, S. E. Bohndiek, and J. Brunker, "Development of a blood oxygenation phantom for photoacoustic tomography combined with online pO2 detection and flow spectrometry," J. Biomed. Opt. **24**(12), 1–11 (2019).
47. I. Hurbain, M. Romao, P. Sextius, E. Bourreau, C. Marchal, F. Bernerd, C. Duval, and G. Raposo, "Melanosome distribution in keratinocytes in different skin types: melanosome clusters are not degradative organelles," J. Invest. Dermatol. **138**(3), 647–656 (2018).
48. H. Y. Thong, S. H. Jee, C. C. Sun, and R. Boissy, "The patterns of melanosome distribution in keratinocytes of human skin as one determining factor of skin colour," Br. J. Dermatol. **149**(3), 498–505 (2003).
49. P. K. Upputuri and M. Pramanik, "Photoacoustic imaging in the second near-infrared window: a review," J. Biomed. Opt. **24**(04), 1 (2019).
50. D. D. Evanoff and G. Chumanov, "Size-controlled synthesis of nanoparticles. 2. Measurement of extinction, scattering, and absorption cross sections," J. Phys. Chem. B **108**(37), 13957–13962 (2004).
51. L. Mohammadi, H. Behnam, J. Tavakkoli, and K. Avanaki, "Skull acoustic aberration correction in photoacoustic microscopy using a vector space similarity model: a proof-of-concept simulation study," Biomed. Opt. Express **11**(10), 5542–5556 (2020).
52. Y.-S. Chen, Y. Zhao, S. J. Yoon, S. S. Gambhir, and S. Emelianov, "Miniature gold nanorods for photoacoustic molecular imaging in the second near-infrared optical window," Nat. Nanotechnol. **14**(5), 465–472 (2019).
53. C. Cai, X. Wang, K. Si, J. Qian, J. Luo, and C. Ma, "Streak artifact suppression in photoacoustic computed tomography using adaptive back projection," Biomed. Opt. Express **10**(9), 4803–4814 (2019).
54. J. S. Turek, M. Elad, and I. Yavneh, "Clutter mitigation in echocardiography using sparse signal separation," >Int. J. Biol. Imaging **2015**, 958963 (2015).
55. G. Matrone, M. A. L. Bell, and A. Ramalli, "Spatial coherence beamforming with multi-line transmission to enhance the contrast of coherent structures in ultrasound images degraded by acoustic clutter," IEEE Transactions on Ultrasonics, Ferroelectrics, and Frequency Control (2021).
56. R. Bulsink, M. Kuniyil Ajith Singh, M. Xavierselvan, S. Mallidi, W. Steenbergen, and K. J. Francis, "Oxygen saturation imaging using LED-based photoacoustic system," Sensors **21**(1), 283 (2021).
57. H.-M. Schwab, M. F. Beckmann, and G. Schmitz, "Photoacoustic clutter reduction using plane wave ultrasound and a linear scatter estimation approach," in *2015 IEEE International Ultrasonics Symposium (IUS)*, (IEEE, 2015), 1–4.
58. M. K. A. Singh and W. Steenbergen, "Photoacoustic-guided focused ultrasound (PAFUSion) for identifying reflection artifacts in photoacoustic imaging," Photoacoustics **3**(4), 123–131 (2015).
59. E. J. Alles, M. Jaeger, and J. C. Bamber, "Photoacoustic clutter reduction using short-lag spatial coherence weighted imaging," in *2014 IEEE International Ultrasonics Symposium*, (IEEE, 2014), 41–44.
60. K. D. Torp, P. Modi, and L. V. Simon, "Pulse oximetry," StatPearls [Internet] (2020).
61. E. M. Coghill, T. Johnson, R. E. Morris, I. L. Megson, and S. J. Leslie, "Radial artery access site complications during cardiac procedures, clinical implications and potential solutions: the role of nitric oxide," WJC **12**(1), 26–34 (2019).
62. J. R. Feiner, J. W. Severinghaus, and P. E. Bickler, "Dark skin decreases the accuracy of pulse oximeters at low oxygen saturation: the effects of oximeter probe type and gender," Anesth. Analg. **105**(6), S18–S23 (2007).
63. L. A. Jensen, J. E. Onyskiw, and N. Prasad, "Meta-analysis of arterial oxygen saturation monitoring by pulse oximetry in adults," Heart & lung **27**(6), 387–408 (1998).
64. P. Clarys, K. Alewaeters, R. Lambrecht, and A. Barel, "Skin color measurements: comparison between three instruments: the Chromameter®, the DermaSpectrometer® and the Mexameter®," Skin Res. Technol. **6**(4), 230–238 (2000).
65. B. O'driscoll, L. Howard, and A. Davison, "BTS guideline for emergency oxygen use in adult patients," Thorax **63**(1), 1–2 (2008).

Biomedical Optics EXPRESS

66. D. Gallagher, S. B. Heymsfield, M. Heo, S. A. Jebb, P. R. Murgatroyd, and Y. Sakamoto, "Healthy percentage body fat ranges: an approach for developing guidelines based on body mass index," Am. J. Clin. Nutr. **72**(3), 694–701 (2000).
67. S. Del Bino and F. Bernerd, "Variations in skin colour and the biological consequences of ultraviolet radiation exposure," Br. J. Dermatol. **169**, 33–40 (2013).